

UNIVERSALITY AND CHAOS IN QUANTUM FIELD THEORIES

B.A. BERG

Department of Physics, The Florida State University, Tallahassee, FL 32306

E. BITTNER, H. MARKUM, R. PULLIRSCH

*Institut für Kernphysik, Technische Universität Wien,
A-1040 Vienna, Austria*

M.-P. LOMBARDO

*Istituto Nazionale di Fisica Nucleare, Laboratori Nazionali del Gran Sasso,
I-67010 Assergi, Italy*

T. WETTIG

*Department of Physics, Yale University, New Haven, CT 06520-8120 and
RIKEN BNL Research Center, Upton, NY 11973-5000*

We investigate the eigenvalue spectrum of the staggered Dirac matrix in SU(3) gauge theory and in full QCD as well as in quenched U(1) theory on various lattice sizes. As a measure of the fluctuation properties of the eigenvalues, we consider the nearest-neighbor spacing distribution, $P(s)$. We further study two-color QCD at nonzero chemical potential, μ , by constructing the spacing distribution of adjacent eigenvalues in the complex plane. We find that in all regions of their phase diagrams, compact lattice gauge theories have bulk spectral correlations given by random matrix theory, which is an indication for quantum chaos. In the confinement phase, the low-lying Dirac spectrum of these quantum field theories is well described by random matrix theory, exhibiting universal behavior.

1 Bulk of the Spectrum

The properties of the eigenvalues of the Dirac operator are of great interest for the universality of certain features of QCD and QED. On the one hand, the accumulation of small eigenvalues is, via the Banks-Casher formula,¹ related to the spontaneous breaking of chiral symmetry. On the other hand, the fluctuation properties of the eigenvalues in the bulk of the spectrum have also attracted attention. It was shown in Ref. 2 that on the scale of the mean level spacing they are described by random matrix theory (RMT). For example, the nearest-neighbor spacing distribution $P(s)$, i.e., the distribution of spacings s between adjacent eigenvalues on the unfolded scale, agrees with the Wigner surmise of RMT. According to the Bohigas-Giannoni-Schmit conjecture,³ quantum systems whose classical counterparts are chaotic have a nearest-neighbor spacing distribution given by RMT whereas systems whose classical counter-

parts are integrable obey a Poisson distribution, $P_{\mathcal{P}}(s) = e^{-s}$. Therefore, the specific form of $P(s)$ is often taken as a criterion for the presence or absence of “quantum chaos”.

In RMT, one has to distinguish several universality classes which are determined by the symmetries of the system. For the case of the QCD Dirac operator, this classification was done in Ref. 4. Depending on the number of colors and the representation of the quarks, the Dirac operator is described by one of the three chiral ensembles of RMT. As far as the fluctuation properties in the bulk of the spectrum are concerned, the predictions of the chiral ensembles are identical to those of the ordinary ensembles.⁵ In Ref. 2, the Dirac matrix was studied for color-SU(2) using both staggered and Wilson fermions which correspond to the chiral symplectic (chSE) and orthogonal (chOE) ensemble, respectively. Here,⁶ we study SU(3) with staggered fermions which corresponds to the chiral unitary ensemble (chUE). The RMT result for the nearest-neighbor spacing distribution can be expressed in terms of so-called prolate spheroidal functions, see Ref. 7. A very good approximation to $P(s)$ is provided by the Wigner surmise for the unitary ensemble,

$$P_W(s) = \frac{32}{\pi^2} s^2 e^{-4s^2/\pi}. \quad (1)$$

We generated gauge field configurations using the standard Wilson plaquette action for SU(3) with and without dynamical fermions in the Kogut-Susskind prescription. We have worked on a $6^3 \times 4$ lattice with various values of the inverse gauge coupling $\beta = 6/g^2$ both in the confinement and deconfinement phase. We typically produced 10 independent equilibrium configurations for each β . Because of the spectral ergodicity property of RMT one can replace ensemble averages by spectral averages if one is only interested in bulk properties.

The Dirac operator, $\not{D} = \not{\partial} + ig\not{A}$, is anti-Hermitian so that the eigenvalues λ_n of $i\not{D}$ are real. Because of $\{\not{D}, \gamma_5\} = 0$ the nonzero λ_n occur in pairs of opposite sign. All spectra were checked against the analytical sum rules $\sum_n \lambda_n = 0$ and $\sum_{\lambda_n > 0} \lambda_n^2 = 3V$, where V is the lattice volume. To construct the nearest-neighbor spacing distribution from the eigenvalues, one first has to “unfold” the spectra.⁷

Figure 1 compares $P(s)$ of full QCD with $N_f = 3$ flavors and quark mass $ma = 0.05$ to the RMT result. In the confinement as well as in the deconfinement phase we observe agreement with RMT up to very high β (not shown). The observation that $P(s)$ is not influenced by the presence of dynamical quarks is expected from the results of Ref. 5, which apply to the case of massless quarks. Our results, and those of Ref. 2, indicate that massive dynamical quarks do not affect $P(s)$ either.

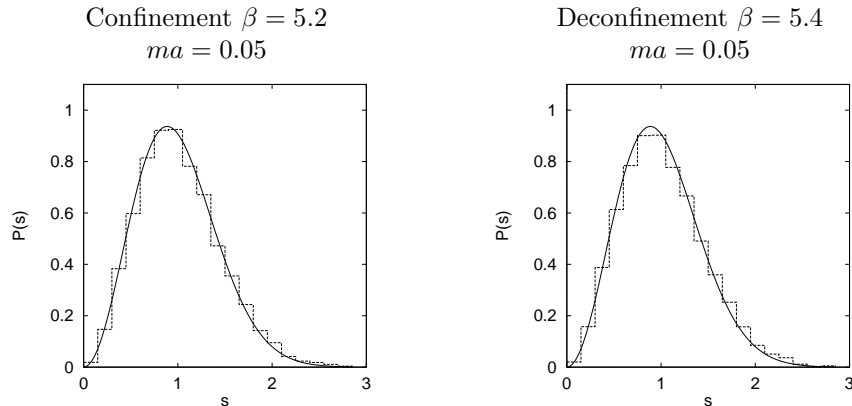


Figure 1: Nearest-neighbor spacing distribution $P(s)$ on a $6^3 \times 4$ lattice in full QCD (histograms) compared with the random matrix result (solid lines). There are no changes in $P(s)$ across the deconfinement phase transition.

No signs for a transition to Poisson regularity are found. The deconfinement phase transition does not seem to coincide with a transition in the spacing distribution. For very large values of β far into the deconfinement region, the eigenvalues start to approach the degenerate eigenvalues of the free theory, given by $\lambda^2 = \sum_{\mu=1}^4 \sin^2(2\pi n_{\mu}/L_{\mu})/a^2$, where a is the lattice constant, L_{μ} is the number of lattice sites in the μ -direction, and $n_{\mu} = 0, \dots, L_{\mu} - 1$. In this case, the spacing distribution is neither Wigner nor Poisson. It is possible to lift the degeneracies of the free eigenvalues using an asymmetric lattice where L_x, L_y , etc. are relative primes and, for large lattices, the distribution is then Poisson, $P_P(s) = e^{-s}$, see Fig. 2.

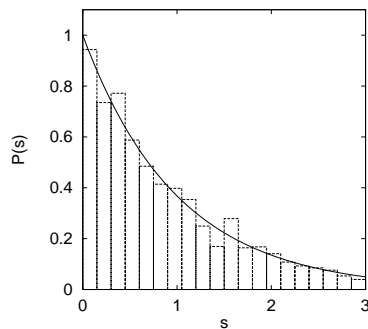


Figure 2: Nearest-neighbor spacing distribution $P(s)$ for the free Dirac operator on a $53 \times 47 \times 43 \times 41$ lattice compared with a Poisson distribution, e^{-s} .

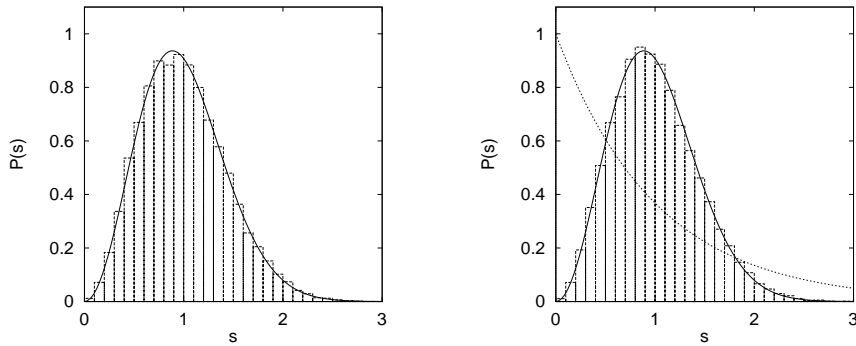


Figure 3: Nearest-neighbor spacing distribution $P(s)$ for U(1) gauge theory on an $8^3 \times 6$ lattice in the confined phase (left) and in the Coulomb phase (right). The theoretical curves are the chUE result, Eq. (1), and the Poisson distribution, $P_P(s) = \exp(-s)$.

We have also investigated the staggered Dirac spectrum of 4d U(1) gauge theory which corresponds to the chUE of RMT but had not been studied before in this context. At $\beta_c \approx 1.01$ U(1) gauge theory undergoes a phase transition between a confinement phase with mass gap and monopole excitations for $\beta < \beta_c$ and the Coulomb phase which exhibits a massless photon for $\beta > \beta_c$.⁸ As for SU(2) and SU(3) gauge groups, we expect the confined phase to be described by RMT, whereas free fermions are known to yield the Poisson distribution (see Fig. 2). The question arose whether the Coulomb phase would be described by RMT or by the Poisson distribution.⁹ The nearest-neighbor spacing distributions for an $8^3 \times 6$ lattice at $\beta = 0.9$ (confined phase) and at $\beta = 1.1$ (Coulomb phase), averaged over 20 independent configurations, are depicted in Fig. 3. Both are well described by the chUE of RMT.

Physical systems which are described by non-Hermitian operators have attracted a lot of attention recently, among others QCD at nonzero chemical potential μ .¹⁰ A formulation of the QCD Dirac operator at $\mu \neq 0$ on the lattice in the staggered scheme is given by¹¹

$$\begin{aligned}
 M_{x,y}(U, \mu) = & \frac{1}{2a} \sum_{\nu=\hat{x},\hat{y},\hat{z}} [U_\nu(x)\eta_\nu(x)\delta_{y,x+\nu} - \text{h.c.}] \\
 & + \frac{1}{2a} [U_{\hat{t}}(x)\eta_{\hat{t}}(x)e^\mu\delta_{y,x+\hat{t}} - U_{\hat{t}}^\dagger(y)\eta_{\hat{t}}(y)e^{-\mu}\delta_{y,x-\hat{t}}] \quad (2)
 \end{aligned}$$

with the link variables U and the staggered phases η . For $\mu > 0$, the Dirac operator loses its Hermiticity properties so that its eigenvalues become complex. The aim of the present analysis is to investigate whether non-Hermitian

RMT is able to describe the fluctuation properties of the complex eigenvalues of the QCD Dirac operator. The eigenvalues are generated on the lattice for various values of μ . We apply a two-dimensional unfolding procedure¹² to separate the average eigenvalue density from the fluctuations and construct the nearest-neighbor spacing distribution, $P(s)$, of adjacent eigenvalues in the complex plane. Adjacent eigenvalues are defined to be the pairs for which the Euclidean distance in the complex plane is smallest. The data are then compared to analytical predictions of the Ginibre ensemble¹³ of non-Hermitian RMT, which describes the situation where the real and imaginary parts of the strongly correlated eigenvalues have approximately the same average magnitude. In the Ginibre ensemble, the average spectral density is already constant inside a circle and zero outside. In this case, unfolding is not necessary, and $P(s)$ is given by¹⁴

$$P_G(s) = c p(cs), \quad p(s) = 2s \lim_{N \rightarrow \infty} \left[\prod_{n=1}^{N-1} e_n(s^2) e^{-s^2} \right] \sum_{n=1}^{N-1} \frac{s^{2n}}{n! e_n(s^2)}, \quad (3)$$

where $e_n(x) = \sum_{m=0}^n x^m/m!$ and $c = \int_0^\infty ds s p(s) = 1.1429\dots$. For uncorrelated eigenvalues in the complex plane, the Poisson distribution becomes¹⁴

$$P_{\mathbb{P}}(s) = \frac{\pi}{2} s e^{-\pi s^2/4}. \quad (4)$$

This should not be confused with the Wigner distribution (1).

We report on simulations done with gauge group $SU(2)$ on a 6^4 lattice using $\beta = 4/g^2 = 1.3$ in the confinement region for $N_f = 2$ flavors of staggered fermions of mass $ma = 0.07$. For this system the fermion determinant is real and lattice simulations become feasible.¹⁵ We sampled 160 independent configurations. In the case of color- $SU(2)$, the staggered Dirac operator has an extra anti-unitary symmetry¹⁶ and falls in the symmetry class with Dyson parameter $\beta_D = 4$.¹⁷ However, one can show that the nearest-neighbor spacing distribution in the bulk of the spectrum is also given by Eq. (3).

Our results for $P(s)$ are presented in Fig. 4. As a function of μ , we expect to find a transition from Wigner to Ginibre behavior in $P(s)$. This was clearly seen in color- $SU(3)$ with $N_f = 3$ flavors and quenched chemical potential,¹² where differences between both curves are more pronounced. For the symplectic ensemble of color- $SU(2)$ with staggered fermions, the Wigner and Ginibre distributions are very close to each other and thus harder to distinguish. They are reproduced by our preliminary data for $\mu = 0$ and $\mu = 0.4$, respectively.

For $\mu > 1.0$, the lattice results for $P(s)$ deviate substantially from the Ginibre distribution and could be interpreted as Poisson behavior, corresponding

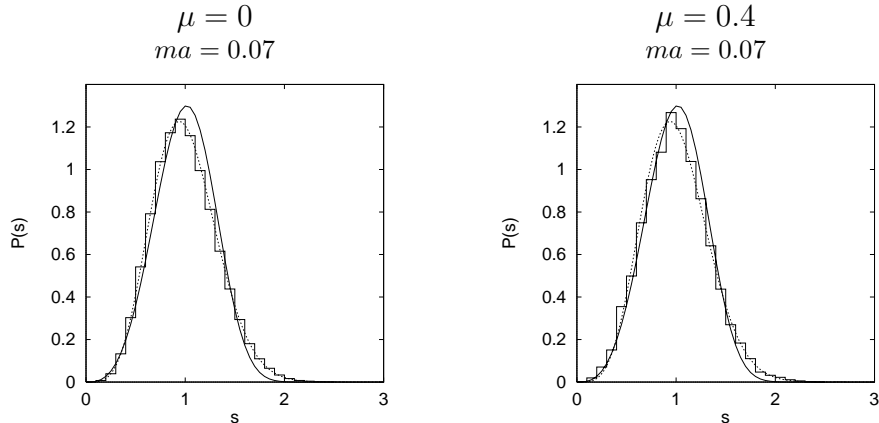


Figure 4: Nearest-neighbor spacing distribution in the complex plane for two-color QCD with μ in the confinement (left) and deconfinement (right) phase. The short-dashed curve is the Wigner distribution for the chSE and the solid curve is the Ginibre distribution of Eq. (3).

to uncorrelated eigenvalues. (In the Hermitian case at nonzero temperature, lattice simulations only show a transition to Poisson behavior for $\beta \rightarrow \infty$ when the physical box size shrinks and the theory becomes free.⁶) A plausible explanation of the transition to Poisson behavior is provided by the following two (related) observations. First, for large μ the terms containing e^μ in Eq. (2) dominate the Dirac matrix, giving rise to uncorrelated eigenvalues. Second, for large μ the fermion density on the finite lattice reaches saturation due to the limited box size and the Pauli exclusion principle.

2 Low-lying Spectrum

We have continued our investigations with a study of the distribution of the small eigenvalues in the confined phase. The Banks-Casher formula¹ relates the Dirac eigenvalue density $\rho(\lambda)$ at $\lambda = 0$ to the chiral condensate, $\Sigma \equiv |\langle \bar{\psi}\psi \rangle| = \lim_{\varepsilon \rightarrow 0} \lim_{V \rightarrow \infty} \pi \rho(\varepsilon)/V$. The microscopic spectral density, $\rho_s(z) = \lim_{V \rightarrow \infty} \rho(z/V\Sigma)/V\Sigma$, should be given by the appropriate result of RMT¹⁸, which also generates the Leutwyler-Smilga sum rules.¹⁹

To study the smallest eigenvalues, spectral averaging is not possible, and one has to produce large numbers of configurations. We present results from Ref. 20 for SU(2) theory and the staggered Dirac operator. Both the distribution $P(\lambda_{\min})$ of the smallest eigenvalue and the microscopic spectral density $\rho_s(z)$ agree with the RMT predictions of the chSE for topological charge $\nu = 0$,

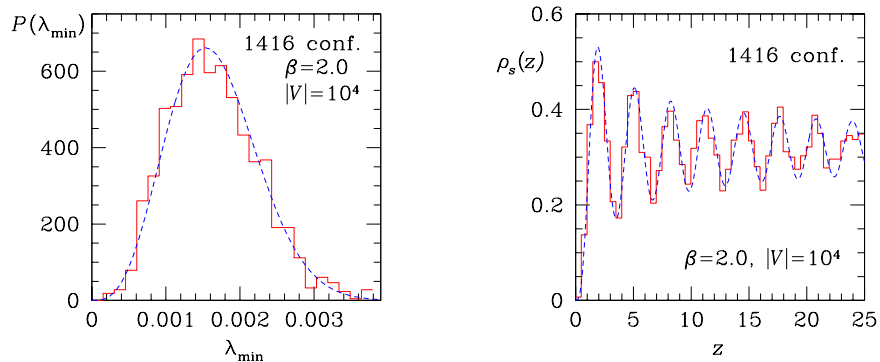


Figure 5: Distribution $P(\lambda_{\min})$ (left) and microscopic spectral density $\rho_s(z)$ (right) from Ref. 20 for SU(2) gauge theory on a 10^4 lattice in comparison with the predictions of the chSE of RMT (dashed lines).

as depicted in Fig. 5.

Our analog results for U(1) theory are for $\beta = 0.9$ in the confined phase with 10000 configurations on a 6^4 lattice. The left plot in Fig. 6 exhibits the distribution $P(\lambda_{\min})$ of the smallest eigenvalue in comparison with the prediction of the (quenched) chUE of RMT for topological charge $\nu = 0$, $P(\lambda_{\min}) = (V\Sigma)^2(\lambda_{\min}/2) \exp(-V\Sigma\lambda_{\min})^2/4$. For the chiral condensate we obtain $\Sigma \approx 0.35$ by extrapolating the histogram for $\rho(\lambda)$ to $\lambda = 0$ and using the Banks-Casher relation. In the right plot of Fig. 6 the same comparison

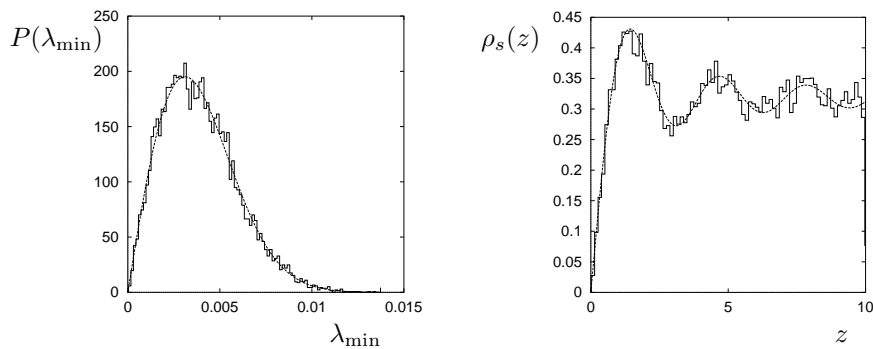


Figure 6: Distribution $P(\lambda_{\min})$ (left) and microscopic spectral density $\rho_s(z)$ (right) from our 6^4 lattice data of U(1) gauge theory in comparison with the predictions of the chUE of RMT (dashed lines).

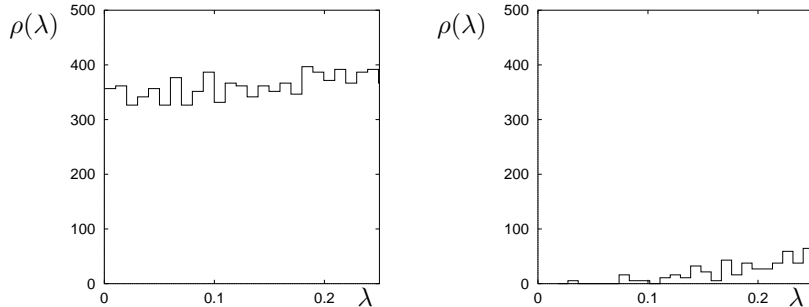


Figure 7: Density $\rho(\lambda)$ of small eigenvalues for U(1) on an $8^3 \times 6$ lattice at $\beta = 0.9$ (left) and at $\beta = 1.1$ (right). A nonzero chiral condensate is supported in the confinement phase of U(1) gauge theory.

with RMT is done for the microscopic spectral density $\rho_s(z)$ up to $z = 10$, and the agreement is again quite satisfactory. Here, the analytical RMT result for the (quenched) chUE and $\nu = 0$ is given by¹⁸ $\rho_s(z) = z [J_0^2(z) + J_1^2(z)]/2$, where J denotes the Bessel function.

In U(1) theory, the quasi-zero modes which are responsible for the chiral condensate $\Sigma \approx 0.35$ build up when we cross from the Coulomb into the confined phase. For our $8^3 \times 6$ lattice, Fig. 7 compares on identical scales densities of the small eigenvalues at $\beta = 0.9$ and at $\beta = 1.1$, averaged over 20 configurations. The quasi-zero modes in the left plot are related to the nonzero chiral condensate, whereas no such quasi-zero modes are found in the Coulomb phase. It would be worthwhile to understand the physical origin of the U(1) quasi-zero modes in more detail. For 4d SU(2) and SU(3) gauge theories a general interpretation is to link them, and hence the chiral condensate, to the existence of instantons. In 4d U(1) gauge theory it has been shown numerically that the chiral condensate is mainly due to monopole configurations.²¹

For two-color QCD, numerical simulations of the full theory with chemical potential in Ref. 15 have exhibited a chiral phase transition at $\mu_c \approx 0.3$ where the chiral condensate as the associated order parameter vanishes. In Fig. 8 we compare the densities of the small eigenvalues at $\mu = 0$ and at $\mu = 0.1$ to 0.4 on our 6^4 lattice, averaged over 160 configurations. Since the eigenvalues move into the complex plane for $\mu > 0$, a band of width $\epsilon = 0.015$ parallel to the imaginary axis is considered to construct $\rho(y)$, i.e. $\rho(y) \equiv \int_{-\epsilon}^{\epsilon} dx \rho(x, y)$, where $\rho(x, y)$ is the density of the complex eigenvalues $x + iy$.

Another interesting question concerns the energy scale E_c up to which RMT describes the small Dirac eigenvalues in the phase where $\Sigma > 0$. In

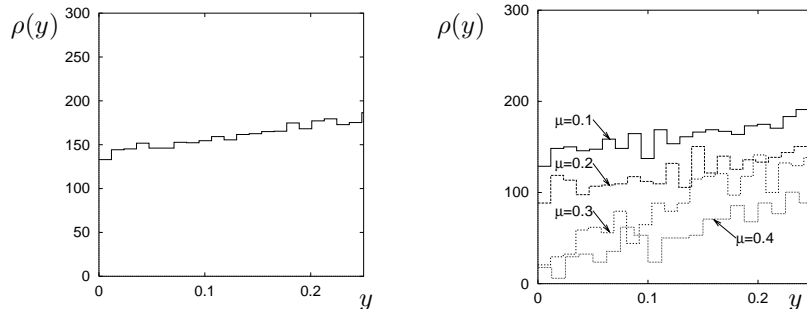


Figure 8: Density $\rho(y)$ of small eigenvalues (see text) for two-color QCD on a 6^4 lattice at $\mu = 0$ (left) and at $\mu = 0.1$ to 0.4 (right). The vanishing of the chiral condensate in the matter phase, found in Ref. 15 at $\mu_c \approx 0.3$, is accompanied by a loss of quasi-zero modes.

disordered mesoscopic systems, a similar scale is called the Thouless energy. The theoretical prediction for QCD is $E_c \sim f_\pi^2 / \Sigma L_s^2$ (see Ref. 22) with the pion decay constant f_π , where we have assumed that the spatial extent L_s of the lattice is not smaller than the temporal extent L_t . In units of the mean level spacing $\Delta = \pi / V \Sigma$ at the origin, this becomes

$$u_c \equiv \frac{E_c}{\Delta} \sim \frac{1}{\pi} f_\pi^2 L_s L_t. \quad (5)$$

A convenient quantity from which u_c can be extracted is the disconnected scalar susceptibility,

$$\chi_{\text{latt}}^{\text{disc}}(m) = \frac{1}{N} \left\langle \sum_{k,l=1}^N \frac{1}{(i\lambda_k + m)(i\lambda_l + m)} \right\rangle_A - \frac{1}{N} \left\langle \sum_{k=1}^N \frac{1}{i\lambda_k + m} \right\rangle_A^2. \quad (6)$$

The corresponding RMT result for the quenched chSE with $\nu = 0$ is given by²³ $\chi_{\text{RMT}}^{\text{disc}} = 4u^2 \int_0^1 ds s^2 K_0(2su) \int_0^1 dt I_0(2stu) \{s(1-t^2) + 4K_0(2u)[I_0(2su) + tI_0(2stu)] - 8stI_0(2stu)K_0(2su)\} - 4u^2 K_0^2(2u) [\int_0^1 ds I_0(2su)]^2$, and for the quenched chUE with $\nu = 0$ we have²⁴ $\chi_{\text{RMT}}^{\text{disc}} = u^2 [K_1^2(u) - K_0^2(u)][I_0^2(u) - I_1^2(u)]$. Here, $u = mV\Sigma$, and I and K are modified Bessel functions. In Figs. 9 and 10 we have plotted the ratio²³

$$\text{ratio} = (\chi_{\text{latt}}^{\text{disc}} - \chi_{\text{RMT}}^{\text{disc}}) / \chi_{\text{RMT}}^{\text{disc}} \quad (7)$$

versus u and $u/(L_s L_t)$, for color-SU(2) with staggered Dirac operator at $\beta = 2.0$ from Ref. 23 and for the U(1) data computed at $\beta = 0.9$, respectively. This ratio should deviate from zero above the Thouless scale. The expected scaling of the Thouless energy with $L_s L_t$ is confirmed.

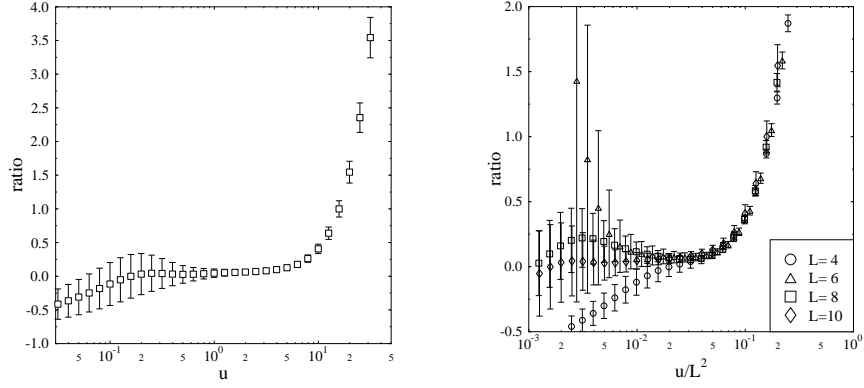


Figure 9: The ratio of Eq. (7) for SU(2) gauge theory plotted versus u and $u/(L_s L_t)$, respectively (in this case, $L_s = L_t = L$). The left plot is for $L = 10$. In the right plot, the data for different L fall on the same curve, confirming the expected scaling of the Thouless energy according to Eq. (5). The deviations of the ratio from zero for very small values of u are well-understood artifacts of the finite lattice size and of finite statistics.²³

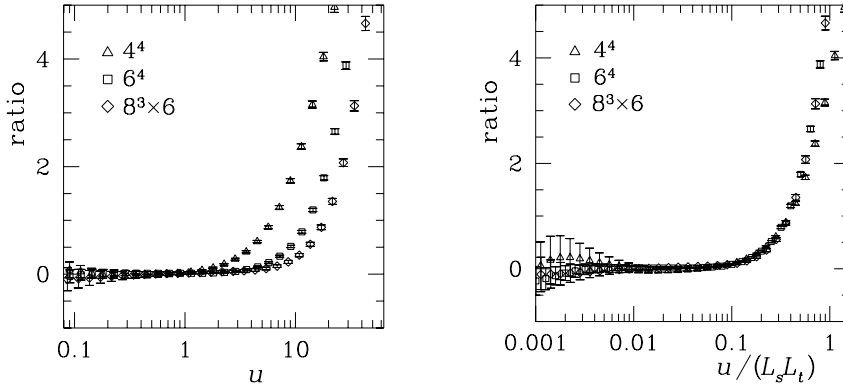


Figure 10: Same as Fig. 9 but for U(1) gauge theory.

3 Conclusions

The aim of this paper was to work out two different types of universalities inherent in quantum field theories and their interpretation in terms of RMT. The first type concerns the bulk of the spectrum of the Dirac operator. The nearest-neighbor spacing distribution $P(s)$ agrees with the RMT result in both the confinement and the deconfinement phase of pure gauge theory and of full QCD, except for extremely large values of β where the eigenvalues are known analytically. The nearest-neighbor spacing distribution of 4d U(1) quenched lattice gauge theory is described by the chUE of RMT in both the confinement and the Coulomb phase. Even in the Coulomb as well as in the deconfinement phase, gauge fields retain a considerable degree of randomness, which apparently gives rise to quantum chaos in these theories.

A general unfolding procedure for the spectra of non-Hermitian operators was applied to the lattice Dirac operator for two-color QCD at nonzero chemical potential. Agreement of the nearest-neighbor spacing distribution in the complex plane with predictions of the Ginibre ensemble of non-Hermitian RMT was found around $\mu = 0.4$. The changes for larger values of μ toward a Poisson distribution are understood formally. The physical interpretation requires a better understanding of QCD at nonzero density.

The second type of universality concerns the low-lying spectra of the Dirac operators of both QCD and QED. In all cases considered, one finds that in the phase in which chiral symmetry is spontaneously broken the distribution $P(\lambda_{\min})$ and the microscopic spectral density $\rho_s(z)$ are described by RMT. The Thouless energy scales with the lattice size as expected.

In summary, both the bulk and the low-lying Dirac spectrum are governed by RMT and the related symmetries.

4 Acknowledgments

This study was supported in part by FWF project P11456-PHY, by DOE contracts DE-FG02-97ER41022, DE-FG05-85ER2500, DE-FG02-91ER40608, and DE-AC02-98CH10886, and by the RIKEN BNL Research Center.

1. T. Banks and A. Casher, Nucl. Phys. B 169 (1980) 103.
2. M.A. Halasz and J.J.M. Verbaarschot, Phys. Rev. Lett. 74 (1995) 3920; M.A. Halasz, T. Kalkreuter, and J.J.M. Verbaarschot, Nucl. Phys. B (Proc. Suppl.) 53 (1997) 266.
3. O. Bohigas, M.-J. Giannoni, and C. Schmit, Phys. Rev. Lett. 52 (1984) 1.
4. J.J.M. Verbaarschot, Phys. Rev. Lett. 72 (1994) 2531.

5. D. Fox and P.B. Kahn, Phys. Rev. 134 (1964) B1151; T. Nagao and M. Wadati, J. Phys. Soc. Jpn. 60 (1991) 3298; 61 (1992) 78; 61 (1992) 1910.
6. R. Pullirsch et al., Phys. Lett. B 427 (1998) 119.
7. M.L. Mehta, *Random Matrices*, 2nd ed. (Academic Press, San Diego, 1991).
8. B.A. Berg and C. Panagiotakopoulos, Phys. Rev. Lett. 52 (1984) 94.
9. B.A. Berg, H. Markum, and R. Pullirsch, Phys. Rev. D 59 (1999) 097504.
10. M.A. Stephanov, Phys. Rev. Lett. 76 (1996) 4472.
11. P. Hasenfratz and F. Karsch, Phys. Lett. B 125 (1983) 308; J.B. Kogut et al., Nucl. Phys. B 225 (1983) 93; I.M. Barbour, Nucl. Phys. B (Proc. Suppl.) 26 (1992) 22.
12. H. Markum, R. Pullirsch, and T. Wettig, Phys. Rev. Lett. 83 (1999) 484.
13. J. Ginibre, J. Math. Phys. 6 (1965) 440.
14. R. Grobe, F. Haake, and H.-J. Sommers, Phys. Rev. Lett. 61 (1988) 1899.
15. S. Hands et al., Nucl. Phys. B 558 (1999) 327.
16. S. Hands and M. Teper, Nucl. Phys. B 347 (1990) 819.
17. M.A. Halasz, J.C. Osborn, and J.J.M. Verbaarschot, Phys. Rev. D 56 (1997) 7059.
18. E.V. Shuryak and J.J.M. Verbaarschot, Nucl. Phys. A 560 (1992) 306; J.J.M. Verbaarschot and I. Zahed, Phys. Rev. Lett. 70 (1993) 3852.
19. H. Leutwyler and A.V. Smilga, Phys. Rev. D 46 (1992) 5607.
20. M.E. Berbenni-Bitsch et al., Phys. Rev. Lett. 80 (1998) 1146.
21. T. Bielefeld et al., Phys. Lett. B 416 (1998) 150.
22. J.C. Osborn and J.J.M. Verbaarschot, Nucl. Phys. B 525 (1998) 738; Phys. Rev. Lett. 81 (1998) 268; R.A. Janik et al., Phys. Rev. Lett. 81 (1998) 264.
23. M.E. Berbenni-Bitsch et al., Phys. Lett. B 438 (1998) 14.
24. M. Göckeler et al., Phys. Rev. D 59 (1999) 094503.